





Are CLIP features all you need for Universal Synthetic Image Origin Attribution?

Dario Cioni^{1,3}, Christos Tzelepis², Lorenzo Seidenari¹, and Ioannis Patras³

¹ University of Florence

² City, University of London

³ Queen Mary, University of London

Abstract. The steady improvement of Diffusion Models for visual synthesis has given rise to many new and interesting use cases of synthetic images but also has raised concerns about their potential abuse, which poses significant societal threats. To address this, fake images need to be detected and attributed to their source model, and given the frequent release of new generators, realistic applications need to consider an Open-Set scenario where some models are unseen at training time. Existing forensic techniques are either limited to Closed-Set settings or to GAN-generated images, relying on fragile frequency-based “fingerprint” features. By contrast, we propose a simple yet effective framework that incorporates features from large pre-trained foundation models to perform Open-Set origin attribution of synthetic images produced by various generative models, including Diffusion Models. We show that our method leads to remarkable attribution performance, even in the low-data regime, exceeding the performance of existing methods and generalizes better on images obtained from a diverse set of architectures. We make the code publicly available at: <https://github.com/ciodar/UniversalAttribution>.

Keywords: Open Set Origin Attribution · Diffusion Models · Deepfake Detection · Open Set Recognition

1 Introduction

Recent generative models can generate synthetic media of exceptional quality and diversity [16, 23, 44], allowing the use of AI-Generated Content (AIGC) in a wide range of areas, such as medical image analysis [42, 46, 59, 76], face reenactment [3–6], image editing [20, 50–52, 61, 62], face anonymization [2], art [11], and fashion [45]. However, alongside their benefits, the broad adoption of AIGC tools raises critical concerns about negative social impacts, including the exploitation of AIGC under malicious intent or towards intellectual property (IP) infringement. That is, users equipped with such powerful and readily available generative models can generate images with biased or inappropriate content and distribute them across digital platforms. Moreover, the unauthorized exploitation of generative models – where model parameters are illicitly obtained and utilized for

unintended commercial purposes – poses a significant challenge to IP protection. Addressing the above problems requires the ability to i) detect synthetic content and ii) trace its provenance to the specific generative model responsible for its creation – this task is typically referred to as *attribution* [8, 68, 69].

Whilst recent generative models span a wide range of architectures, they can be categorized into the following three major classes: i) Variational Autoencoders (VAEs) [55], ii) Generative Adversarial Networks (GANs) [7], and iii) Diffusion Models (DMs) [23]. The attribution problem has mainly been studied in the case of GANs, where GAN-generated images are attempted to be attributed to the specific GAN architecture that gave rise to them. For doing so, early works (e.g., [43]) relied on distinctive residual features, typically referred to as *fingerprints*, that are inherited in the image during the generation process, and which can be extracted by performing a frequency transformation of the image [43, 70]. Further research in GAN attribution [22, 25, 73] validated the existence of such fingerprints, allowing to identify the generator among a finite, fixed (i.e., closed) set of models. Albeit, the fast progress and the rapid introduction of new generative models (both under the GAN- and diffusion-based paradigms) greatly limits the applicability of such closed-set setting. A few recent works in GAN attribution addressed this limitation by allowing the attribution at an architecture-level [8, 68] or by adopting an Open Set Recognition approach [69]. However, such methods do not take into account diffusion-based generative models, which have emerged as the leading generative paradigm, whilst at the same time the adopted fingerprints used to perform attribution can be catastrophically affected by perturbations introduced during common content-sharing stages (e.g., uploading to content sharing platforms), such as JPEG compression and resizing. Finally, these works typically rely on costly optimization of specialized deep networks, which need thousands of samples per class to obtain acceptable results.

In this work, we adopt a forensic approach to address the above limitations of state-of-the-art works by considering the fragility of fingerprint-based approaches and the urge to address the problem in a realistic Open-Set scenario. More specifically, we take a different angle to the problem shifting from low-level, frequency-based representations to higher-level image features. Motivated by the generality and expressiveness of the representations of modern foundation multimodal models (e.g., DINOv2 [53] and CLIP [54]) that have been trained on extremely large dataset (i.e., LVD-142M [53], LAION-2B [57], WIT400M [54], Datacomp-1B [27], and YMFCC [60]), we show that by using an intermediate feature representation scheme, we can obtain a sufficiently general representation to address synthetic image attribution in open-set scenarios. Moreover, we show that not learning the representation with an inductive bias derived by a single class of models (e.g., as in [69]) allows for detection and attribution on a more diverse set of data. Specifically, detecting synthetic images coming from different families of models and datasets. Finally, by contrast to methods that rely on model parameters (which may not be accessible), we operate in a realistic open-set setting. Our contributions can be summarized as follows:

- We explore the Open-Set model attribution of diffusion-generated images and we show that our method generalizes to diffusion-generated images much better than recent Open-Set attribution techniques (i.e., [8, 68, 69]) proposed for GAN-generated images.
- We propose a novel framework for the Open-Set diffusion-based model attribution task inspired by Open Set Recognition [63], employing a recently released large-scale dataset comprising several Diffusion Models.
- We show that the proposed learning framework that incorporates features extracted from foundation models (i.e., CLIP [54] and DINOv2 [53]) exceeds the performance of existing methods, even in the low-data regime, and generalizes better on images obtained from a diverse set of architectures in comparison to most of the existing works.

2 Related work

Attribution of synthetic images Attribution of synthetic images consists in assigning any given synthetic image to the generative model that produced it. Certain lines of research address this task by actively embedding a signal during the generation process [24, 35, 71, 72], by performing inverse engineering [36, 41, 56, 65], or by conducting a forensic examination on the images [8, 22, 26, 28, 43, 68–70]. The latter (i.e., the *forensic approach*) typically leads to greater flexibility, as it does not require access to the generative models (which may not be accessible). Forensic techniques used for attribution of GAN-generated images rely on unique residual patterns inherited by those generative models on the image (i.e., *fingerprints*), which can be better analyzed by observing the frequency spectrum [22, 26, 43]. However, such methods do not address diffusion-based generative models, which have emerged as the leading generative paradigm recently, whilst at the same time the adopted fingerprints used to perform attribution can be catastrophically affected by perturbations introduced during common content sharing stages (e.g., uploading to content sharing platforms), such as JPEG compression and resizing. By contrast, in this work we propose a general framework that addresses both Diffusion- and GAN-based attribution and does not suffer from fragile low-level frequency artifacts.

Moreover, most existing works focus on a closed-set classification setting – i.e., attribution is performed on images generated by a fixed and known set of models trained on a specific dataset with a specific seed and loss. This setting poses a significant limitation on the attribution mechanism, since new generative methods become available, while their models might not be open-sourced/available. To address this crucial constraint, a few recent works proposed to perform attribution at an architecture-level [8, 68] or to frame it as an open-set classification task [28, 69]. While these works have shown promising results, they only focus on GAN-generated images. In this work we show that, despite the fact that diffusion-based generation also inherits distinctive fingerprints in the generated images [13], such methods do not generalize to diffusion-based generation [14, 49]. By contrast, our method provides a general

Open-Set [69] attribution framework where, instead of relying on fragile low-level frequency artifacts, we propose to perform attribution leveraging pre-trained features extracted from pre-trained visual encoders of powerful foundation models (i.e., CLIP [54], DINOv2 [53]), which allows for better generalization ability to unseen model categories and a higher robustness to image perturbations.

Foundation models for image forensics While the vast majority of existing works focus address the problem of attribution on GAN-generated images, very recent works extended the analysis to synthetic images generated by Diffusion Models, but only for the simpler binary detection task. To obtain a universal fake image detection system, several works [1, 12, 15, 49, 58, 74] employed features extracted from large pretrained vision or vision-language models such as DINOv2 [53] and CLIP [54], either in a multimodal setting by leveraging a textual prompt in conjunction with the visual information [1, 15, 58], or in a visual-only setting [12, 49]. The feature space is exploited by using k Nearest Neighbors or linear probing approaches similarly to Ojha *et al.* [49] and successive works [1, 12] or by training a deep network, similarly to [74]. However, few works [15, 49, 74] evaluated their performance in the presence of unknown generators by framing the task as an outlier detection problem, and only Sha *et al.* [58] evaluated the possibility of attributing Diffusion-generated images to the model that originated them, but in a limited closed-set comprising four generators. By contrast, in this work, we study the more general Open-Set Attribution setting, leveraging pre-trained features extracted from large vision encoders and focusing on generalization and robustness properties.

3 Proposed Method

In this section, we present our Open-Set model attribution framework. We begin by introducing the problem in Sec. 3.1 and we present our method in Sec. 3.2, where we discuss the proposed feature extraction protocol and the adopted learning approaches. An overview of the proposed method is given in Fig. 1.

3.1 Problem Statement

In this work, we address the problem of synthetic image detection and attribution in the most general setting possible. More specifically, we assume that a certain set $\mathcal{I}_{\mathcal{K}} = \{x_{\mathcal{K}}^1, \dots, x_{\mathcal{K}}^{N_{\mathcal{K}}}\}$ of $N_{\mathcal{K}}$ synthetic and real images are available and that, for each of these images model provenance (in the case of synthetic images) is known. That is, each image $x_i \in \mathcal{I}_{\mathcal{K}}$ is annotated with a label $y_i \in \{\mathcal{R}\} \cup \mathcal{O}_{\mathcal{K}}$, where \mathcal{R} denotes the set of real images, and $\mathcal{O}_{\mathcal{K}} = \{\mathcal{M}_{\mathcal{K}}^1, \dots, \mathcal{M}_{\mathcal{K}}^{N_{\mathcal{O}_{\mathcal{K}}}}\}$ denotes the set of $N_{\mathcal{O}_{\mathcal{K}}}$ known models. Assuming that at any given time a set of $N_{\mathcal{O}_{\mathcal{U}}}$ unknown models $\mathcal{O}_{\mathcal{U}} = \{\mathcal{M}_{\mathcal{U}}^1, \dots, \mathcal{M}_{\mathcal{U}}^{N_{\mathcal{O}_{\mathcal{U}}}}\}$ can be used to generate new images, we take into account another disjoint set of $N_{\mathcal{U}}$ images $\mathcal{I}_{\mathcal{U}} = \{x_{\mathcal{U}}^1, \dots, x_{\mathcal{U}}^{N_{\mathcal{U}}}\}$ generated by those unknown models $\mathcal{O}_{\mathcal{U}}$ – that is, each image $x_i \in \mathcal{I}_{\mathcal{U}}$ is annotated with a label $y_i \in \mathcal{O}_{\mathcal{U}}$ corresponding to the unknown model that produced it.

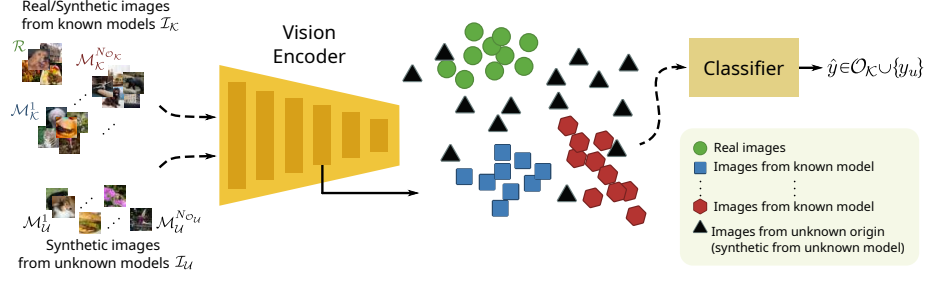


Fig. 1: Overview of the proposed attribution framework – we incorporate intermediate features from the Vision Encoder of a powerful foundation model in order to perform synthetic image detection and attribution. Using real images (from a set \mathcal{R}), synthetic images generated by a set of known generative models $\mathcal{O}_K = \{\mathcal{M}_K^1, \dots, \mathcal{M}_K^{N_{\mathcal{O}_K}}\}$, and synthetic images generated by a set of unknown generative models $\mathcal{O}_U = \{\mathcal{M}_U^1, \dots, \mathcal{M}_U^{N_{\mathcal{O}_U}}\}$, we optimize a classifier to assign images to either a known model from \mathcal{O}_K or “reject” such assignment, classifying the images as *synthetic-and-unknown* (y_u).

Given an image x of unknown provenance, that can be either a real image or a synthetic image generated by a known or unknown model from $\mathcal{O}_K \cup \mathcal{O}_U$, we need to decide on whether this image is real or it has been generated by a generative model. In the latter case, we also need to predict which of the known models \mathcal{O}_K has been used or to “reject” such assignment, classifying the image as *synthetic-and-unknown*, following the common practice in literature [10, 63, 69]. Formally, for each given image x , we predict its class $\hat{y} \in \mathcal{O}_K \cup \{y_u\}$, where y_u is a special class that indicates that the image at hand is neither real nor generated by a known model. We illustrate this process in Fig. 1.

3.2 Open-Set Model Detection and Attribution

Visual backbone and feature extraction In order to extract meaningful features for the task of detection and attribution, as discussed in previous sections, motivated by the generality and expressiveness of the representations of modern foundation multimodal models, we propose to employ the Vision Transformer-based [21] encoder of a foundation model and extract intermediate features, instead of using the final feature representations. More specifically, each image $x \in \mathbf{R}^{C \times H \times W}$ is split into a sequence of square patches $\{x_i^p\}_{i=1}^N$, where C , H , and W denote the channel, width, and height, respectively, and each patch has size $P \times P$. Each patch is then projected into a d -dimensional embedding space, and an additional token [CLS] is concatenated to the input sequence. The embedding sequence is then fed to a Transformer backbone, composed by L transformer blocks, each receiving the output of the previous block. We further detail this process in Sec. 4.1.

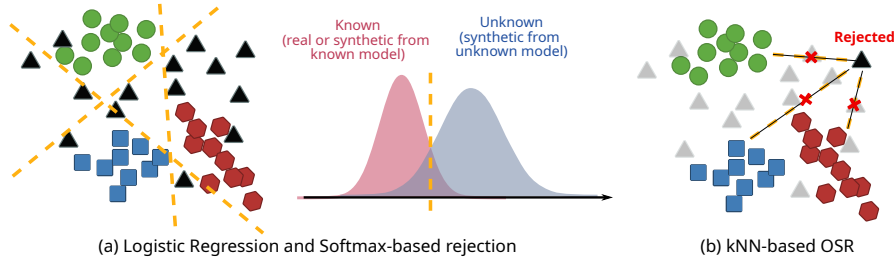


Fig. 2: Proposed learning approach for Open-Set model detection and attribution.

Next, we perform the classification task (of assigning each image to a class in $\mathcal{O}_K \cup \{y_u\}$ – see Fig. 1) following either a *Linear Probe* or a *kNN* approach as described below.

Linear Probe In this approach, we use the extracted features to train a logistic regressor similarly to [54]. By doing so, we identify the block that provides the most informative features, enabling the linear model to classify known and reject unknown models. The logistic regressor is trained with an ℓ_2 loss using an off-the-shelf LBFGS [38] solver. We perform a hyperparameter sweep to determine the optimal value for the regularization parameter for the features of each block. Rejection is performed based on the confidence on the prediction on each sample. This is illustrated in Fig. 2 (a).

k-Nearest-Neighbors (kNN) In this approach, we measure the distances within the visual feature space, extracted by the pre-trained backbones with no further fine-tuning. As the features needed for our task may be significantly different to the original task where the backbone network has been trained for, we additionally evaluate a trained linear projection of the features using the Sup-Con [34] loss for 10 epochs. During validation and testing, the cosine distances between each element and the training features are calculated and each data point is assigned to a specific class by majority voting on the k nearest features in the embedding space. Rejection is performed based on the distance of the nearest neighbor. This is illustrated in Fig. 2 (b).

4 Experiments

In this section we will present the experimental evaluation of the proposed framework. In Sec. 4.1, we will introduce the experimental setup. In Sec. 4.2 present comparisons with several state-of-the-art works, and in Sec. 4.3 we will present ablation studies on various design choices of the proposed framework.

Table 1: Example split of the GenImage [75] dataset similarly to [63, 69].

Image Source	Set	Generator
ImageNet [17]	Seen Real	-
GenImage [75]	Seen Fake	wukong [67] Midjourney [44] SD1.4 [66] VQDM [29]
	Unseen Fake	glide [48] ADM [19] SD1.5 [66] BigGAN [7]

4.1 Experimental setup

Dataset We evaluated the proposed method on the GenImage [75] dataset, originally designed for binary Synthetic Image Detection. This dataset includes real images from ImageNet and synthetic images from eight different conditional generative models, including seven diffusion- and one GAN-based models –namely, Midjourney (MJ) [44], Stable Diffusion V1.5 (SD1.5) [66], Stable Diffusion V1.4 (SD1.4) [66], Wukong [67], VQDM [29], ADM [19], GLIDE [48], and BigGAN [7]. These generative models are either Text-to-Image (MJ, SD, Wukong, VQDM, GLIDE), utilizing ImageNet classes as text prompts, or class-conditional (ADM, BigGAN). The GenImage dataset is split into the following three subsets:

- *Seen Real*: 4K samples of real ImageNet images,
- *Seen Fake*: 16K images produced by generative models included in the training set, and
- *Unseen Fake*: 16K images produced by generative models not included in the training set.

Following the common practice in Open Set Recognition literature [63, 69], we built five different splits of the dataset by varying the models included in *Seen Fake* and *Unseen Fake* subsets. An example of such split is shown in Tab. 1. We provide the details for all five splits in Appendix A.1. In our main experiments we used $n = 4$ models from both *Seen Fake* and *Unseen Fake*. An ablation on the number of n of training classes (models) can be found in Sec. 4.3. We train all competing methods [8, 68, 69] on the five dataset splits and report the average of each metric in the results.

Visual backbones and feature extraction We evaluated two families of backbones pre-trained on large-scale datasets for feature extraction, both adopting the Vision Transformer [21] architecture. The first was trained on a cross-modal setting using the contrastive loss, while the second was trained on a visual-only setting using self-supervision. Specifically, we employed the vision encoder of CLIP [54], using the OpenCLIP⁴ implementation trained on the LAION-2B

⁴ https://github.com/mlfoundations/open_clip

dataset, composed of 2 billion image-text couples collected from the Internet, and DINOv2 [53], which has been pre-trained on the LVD-142M dataset using a self-supervision approach based on image augmentation and enforcing consistency between local and global patches of the image. More specifically, we employed the base version of ViT [21] for all considered backbones, which is composed by $L = 12$ Transformer blocks and 768-dimensional embeddings. The pre-trained visual backbones were used as feature extractors for each image during the training, validation, and testing phases. Each image $x \in \mathbf{R}^{C \times H \times W}$ was split into a sequence of squared patches $\{x_i^p\}_{i=1}^N$, where $C = 3$, $H = 224$ and $W = 224$ are the channel, width, and height, respectively, and each patch has size 16×16 for CLIP and 14×14 for DINOv2. Each patch was then projected into a 768-dimensional embedding and an additional token (i.e., $[CLS]$) was concatenated to the input sequence. The embedding sequence was then fed to a Transformer backbone, composed by $L = 12$ transformer blocks, each receiving the output of the previous block.

Evaluation metrics Following the common practice in the relevant literature, we evaluated the proposed framework using the standard metrics proposed for Open Set Recognition [63] and Open Set Model Attribution [69]. More specifically, we report results on the accuracy on the Closed-Set setting, composed of *Seen Real* and *Seen Fake* images, and on the Area Under the ROC curve (AUROC) on the Open-Set setting, composed of *Seen Real*, *Seen Fake*, and *Unseen Fake* images. The AUROC is a threshold-independent metric that monitors the true positive rate against the false positive rate by varying the rejection threshold, and it can be interpreted as the probability that a positive example is assigned a higher detection score than a negative example.

To balance between the Closed-Set accuracy and the Open-Set rejection, we further employed the Open-Set Classification Rate (OSCR) [18] metric. The OSCR metric is defined using the Correct Classification Rate (CCR), defined as the fraction of examples of *Seen data* \mathcal{D}_S where the correct class \hat{k} has the maximum probability and the probability is greater than a threshold τ ,

$$\text{CCR}(\tau) = \frac{|\{x \mid x \in \mathcal{D}_S \wedge \arg \max_k P(k \mid x) = \hat{k} \wedge P(\hat{k} \mid x) > \tau\}|}{|\mathcal{D}_S|}, \quad (1)$$

and the False Positive Rate (FPR), defined as the fraction of samples from unknown data \mathcal{D}_U that are classified as any known class k with a probability greater than a threshold τ ,

$$\text{FPR}(\tau) = \frac{|\{x \mid x \in \mathcal{D}_U \wedge \max_k P(k \mid x) \geq \tau\}|}{|\mathcal{D}_U|}. \quad (2)$$

The OSCR is then calculated as the area under the curve of the CCR against the FPR metrics. Following the protocol proposed in [47], we report the average over the five splits of the dataset.

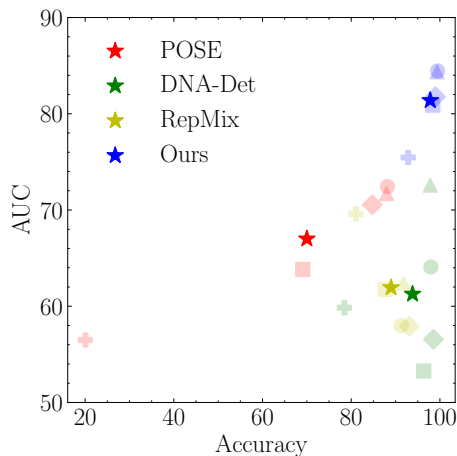


Fig. 3: Comparison with GAN Attribution methods on closed-set performance (Accuracy) and open-set performance (AUROC) on the GenImage [75] dataset. Foreground points in bold show results averaged across five “Seen/Unseen” class splits for each method (following standard practice in the OSR literature), while background points, shown faint, indicate results from the underlying individual splits. Our method outperforms state-of-the-art in both closed-set and open-set performance.

Table 2: Diffusion Models Open Set Origin Attribution on GenImage [75] dataset. We report the Closed-Set Accuracy and Open-Set AUC and OSCR. We report the mean on the five splits of the dataset \pm the standard deviation. The best performance is highlighted in **bold** and second best is underlined.

Method	Acc.	AUC	OSCR
ResNet-50 [30]	91.66 ± 3.74	70.74 ± 5.27	68.29 ± 6.98
ViT [21]	93.26 ± 2.83	67.77 ± 5.58	66.02 ± 7.24
DNA-Det [68]	93.83 ± 7.72	61.27 ± 6.70	75.08 ± 11.02
RepMix [8]	88.98 ± 4.36	61.93 ± 4.26	57.92 ± 1.73
POSE [69]	70.00 ± 25.95	67.00 ± 6.08	53.35 ± 19.82
Ours (NN)	93.26 ± 5.46	77.18 ± 1.88	72.06 ± 3.26
Ours (NN+)	<u>94.59 ± 5.92</u>	<u>80.96 ± 4.85</u>	<u>77.80 ± 9.27</u>
Ours (LP)	97.82 ± 2.51	81.39 ± 3.28	80.78 ± 4.02

4.2 Comparison with state-of-the-art (SOTA) attribution methods

Comparison with SOTA on diffusion-generated images We compare our method with two common baseline architectures, fine-tuned on the GenImage [75] dataset, and existing SOTA methods for GAN Open-Set model attribution, namely, DNA-Det [68], RepMix [8], and POSE [69].

All methods were trained on the GenImage [75] dataset utilizing the publicly available code and the augmentations and data transformations proposed by each method. Fig. 3 highlights that our method demonstrates superior attribution performance both in Closed-Set attribution, assessed by Accuracy, and in the Open-Set, assessed by AUROC.

In Tab. 2 we show the performance comparison between our method and the baselines and SOTA. While DNA-Det [68] and RepMix [8] achieve closed-set accuracy close to or above 90%, their open-set performance is inferior to ours. Conversely, POSE [69] exhibits improved open-set performance compared

Table 3: GAN Open Set Origin Attribution on OSMA [69] dataset. Similar to Tab. 2, we report the Closed-Set Accuracy and Open-Set AUC and OSCR for the unknown data. Results are averaged on the five splits of the dataset. The best performance is highlighted in **bold**, second best is underlined.

Method	Acc.	Unseen Seed		Unseen Arch.		Unseen Data		Unseen All	
		AUC	OSCR	AUC	OSCR	AUC	OSCR	AUC	OSCR
PRNU [43]	55.27	69.20	49.16	70.02	49.49	67.68	48.57	68.94	49.06
Yu <i>et al.</i> [70]	85.71	53.14	50.99	69.04	64.17	78.79	72.20	69.90	64.86
DCT-CNN [26]	86.16	55.46	52.68	72.56	67.43	72.87	67.57	69.46	64.70
DNA-Det [68]	93.56	61.46	<u>59.34</u>	<u>80.93</u>	76.45	66.14	63.27	71.40	68.00
RepMix [8]	93.69	54.70	53.26	72.86	70.49	78.69	76.02	71.74	69.43
POSE [69]	<u>94.81</u>	<u>68.15</u>	67.25	84.17	81.62	88.24	85.64	82.76	80.50
Ours (NN)	94.18	57.62	56.69	77.95	75.16	90.60	91.77	80.42	77.11
Ours (NN+)	95.31	56.18	54.04	80.22	77.27	<u>88.90</u>	85.42	<u>80.65</u>	78.22
Ours (LP)	97.29	54.15	54.00	78.78	<u>78.12</u>	90.60	<u>89.52</u>	79.29	<u>78.77</u>

to other GAN attribution methods, but falls significantly short in closed-set accuracy. In addition, POSE’s training mechanism, based on the interpolation of diverse fingerprints, is fragile to variations of classes seen during training, as highlighted by the high standard deviation. Fine-tuned deep architectures, such as ResNet-50 [30] and ViT [21], show better open-set recognition performance compared to GAN-specific methods, highlighting the low effectiveness of the training techniques proposed in GAN attribution methods when transferred to Diffusion-generated images.

Our approach is in general superior with linear probing (LP) getting the highest gain in term of all three metrics, with gains of 4%, 10%, and 5% in terms of Accuracy, AUC, and OSCR, respectively, with respect to the best SOTA performer for each metric. Moreover, the standard deviation across the splits is lower than the best performing competitor in each setting, showing the robustness of our findings. The incorporation of the SupCon [34] (NN+) yields further improvement for the simpler Nearest Neighbour approach (NN). Simpler baselines, i.e., ResNet-50 and ViT, still obtain competitive results in term of accuracy but fail to deliver performance in the Open-Set scenario, as shown by the AUC and OSCR metrics.

Comparison with SOTA on GAN-generated images To validate the generalization ability of our method in attributing images produced by other classes of models, in Tab. 3 we compare our work against GAN attribution SOTA works on the OSMA [69] dataset, which consists of images generated by several GAN architectures. Although in this setting POSE [69] achieves a better open-set performance, our method achieves a better closed-set accuracy and an open-set performance comparable with other GAN attribution methods. In this setting, the k NN-based approach with a trained linear projection achieves a better AUC,

while the best accuracy and Open-Set OSCR is achieved by linear probe. We provide extended results with standard deviations in Appendix A.3.

4.3 Ablation studies

Architecture We evaluated different architectures as feature extractors for linear probing. For each architecture, we performed a sweep on all available layers, evaluating closed-set and open-set performance. We evaluated five models, all sharing the ViT-B architecture. Namely, the visual encoder of CLIP [54], both in the original and OpenCLIP implementation, DINOv2 [53], DINO [9], and ViT [21]. Results are shown in Fig. 4. Although both CLIP and DINOv2 attain a closed-set accuracy above 95%, they vary greatly in open-set performance, with OpenCLIP reaching the best AUC and OSCR. Using features from the last layer of all models lead to a lower closed-set accuracy, as well as Open-Set performance. Therefore, the choice of the point of the network to be used for feature extraction is important for the final classifier performance, as the backbone will not be fine-tuned for the attribution task. DINOv2 shows the best Open Set performance in the very first layers, and it sharply decreases in successive layers.

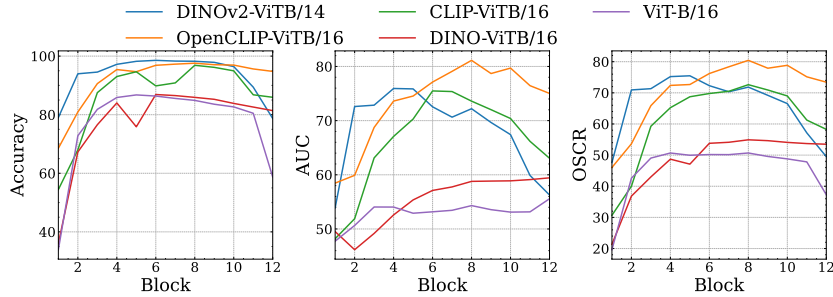


Fig. 4: Comparison of closed-set and Open Set performance on GenImage of a linear probe trained with features extracted from different backbones with the n -th Transformer block of each backbone. Results are averaged across the five splits of the dataset.

Impact of number of training samples We evaluated our approach in the scenario when only a limited number of data samples is available. Specifically, we employed a number ranging from 4K to a few-shot scenario with only 10 samples for each of the 5 known classes of GenImage [75]. We show in Fig. 5 that our method achieves a good OSCR performance even in the most challenging configuration, while POSE’s [69] OSCR score drops to under 20% in this setting. As expected, using pre-trained features from a large-scale model as CLIP provide great data efficiency, requiring only a limited number of data points for training.

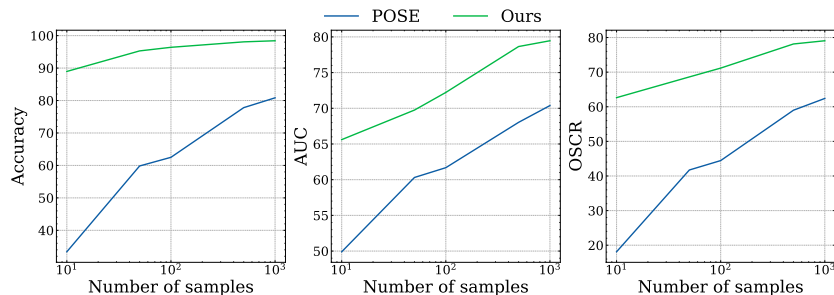


Fig. 5: Closed-Set Accuracy and Open Set performance of classifiers trained on an increasing number of samples per class, ranging from 10 to 4k.

Table 4: Closed-Set Accuracy and Open Set performance of classifiers trained on GenImage [75] when varying the ratio of known and unknown classes. The following scenarios are considered: 2 classes, 4 classes, 6 classes, and 8 classes (close-set only). The best performance is highlighted in **bold**.

Method	2 Classes			4 Classes			6 Classes			8 Classes
	Acc.	AUC	OSCR	Acc.	AUC	OSCR	Acc.	AUC	OSCR	Acc.
RepMix [8]	85.24	65.85	63.40	88.98	61.93	57.92	93.48	66.31	55.44	76.10
POSE [69]	65.51	59.02	41.75	70.00	67.00	53.35	80.93	66.87	61.58	63.39
Ours (LP)	98.40	82.70	82.33	97.82	81.39	80.78	87.71	79.77	73.65	85.54

Number of training classes In Tab. 4 we compare our methods with SOTA when the number of training classes is varied between 2 and 8, with the remaining classes being inserted in the Unknown Fake set. Our method shows a consistent performance in all considered scenarios, while POSE’s [69] performance drops significantly when decreasing the number of training classes to just 2. The Closed-Set setup with 8 generators appears to be the most challenging, as it requires to distinguish models with very similar characteristics (e.g., SDv1.4 and SDv1.5). RepMix [8] also achieves a consistent performance, but shows a lower accuracy and open-set performance. Since our method does not rely on the simulation of diverse fingerprints [69], it performs well even with few classes.

Impact of input perturbations To study the effects of individual perturbations on attribution performance, we evaluated our method, POSE [69] and a baseline fine-tuned ResNet [30] on GenImage [75] images perturbed by applying seven types of perturbations – namely, JPEG Compression, Gaussian Blur, additive Gaussian Noise, Brightness, Contrast, Saturation, and Rotation. In Fig. 6 we give an indicative example of the effect of each perturbation. Each perturbation is applied with an intensity randomly sampled within an interval provided in Appendix A.4, and the methods are immunized by adding the perturbation as augmentation during the training phase. Fig. 7 reports the Closed-Set and Open-Set performance on GenImage [75] under the attacks described above. The

perturbations cause a loss in performance for all methods, with Gaussian Noise and Gaussian Blur impacting the most on our method. All perturbations that alter the structure of the image have the most impact on POSE [69], while color alterations have a reduced impact, which is extremely reduced for our method. Remarkably, JPEG compression causes the least drop in performance in our method, while heavily affecting the existing SOTA methods.

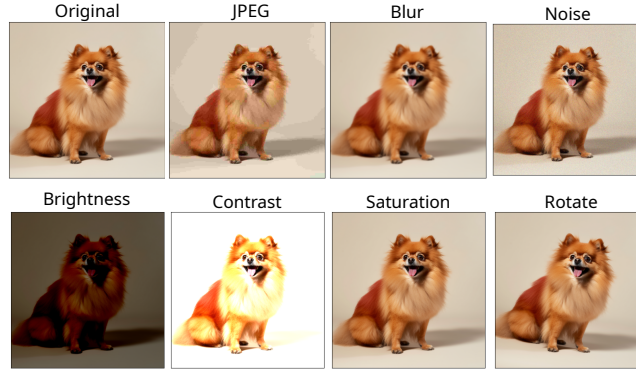


Fig. 6: Visual comparison of common image perturbations applied on a sample image.

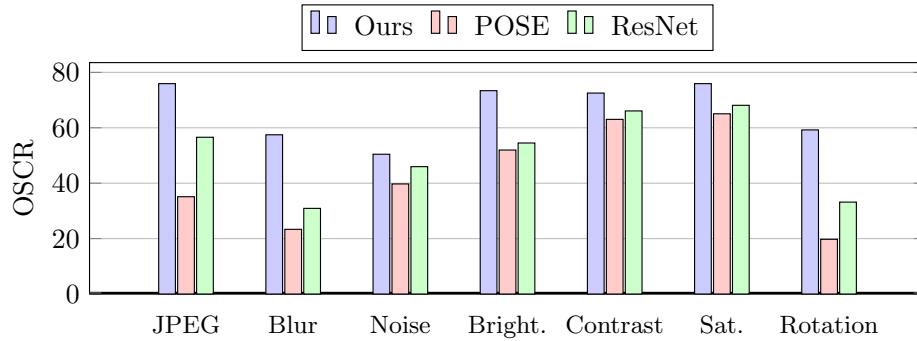


Fig. 7: Robustness to perturbations on GenImage [69] dataset.

Rejection strategy While POSE [69] performs rejection based on the softmax probabilities, designing a proper score function that aims to separate ID from OOD data is essential to perform the rejection of unknown classes successfully. Thus, we further evaluated the Open-Set classification performance when using different rejection strategies, employing both post-hoc methods that rely only

on the predictive distribution, and methods relying on feature statistics calculated from known training data \mathcal{I}_K . We provide details of each rejection strategy in Appendix A.6. In Tab. 5 we show the Open-Set performance, measured by AUC and OSCR, of both post-hoc and methods requiring ID data on GenImage dataset. All post-hoc methods show a better performance than the MSP baseline and the best performing method is GEN [40]. Methods requiring ID features, such as Mahalanobis and Residual, do not show a good performance, as they rely on ID features which are not fine-tuned for the specific task in our linear probing configuration. Overall, the best performing rejection method combines GEN and the Residual feature calculation, which improves over the MSP baseline by 4.5 points in AUROC and 2.5 points in OSCR.

Table 5: Comparison of different rejection strategies on GenImage [69] dataset, either based on post-hoc transformation of the predictive distribution (first part) or on statistics calculated on the known data (second part).

Method	AUC	OSCR
MSP [32]	80.19	78.07
MaxLogit [31]	80.66	78.13
Energy [39]	80.47	77.83
GradNorm [33]	43.92	41.14
Shannon Entropy [40]	80.59	78.31
GEN [40]	80.91	78.41
GEN + Local ReAct [40, 64]	80.91	78.40
Mahalanobis [37]	70.37	65.80
Residual [64]	70.01	65.40
ViM [64]	80.02	77.49
GEN + ReAct [40, 64]	77.19	74.27
GEN + Residual [40]	84.87	80.66

5 Conclusion

In this paper, we presented our method for Open-Set synthetic image detection and attribution based on foundation models. Our in-depth comparison shows that CLIP features are extremely effective in open-set attribution scenarios, while previously proposed models are designed to recognize GAN-originated signatures, which leads to reduced performance on diffusion-generated images. Moreover, CLIP performs best independently from the number of classes to be recognized in the known set and outperforms competing methods in the few-shot scenario. Finally, we analyze the robustness of our method when common image perturbations are applied. In this scenario, when immunization is provided, our method is still performing better than existing methodologies.

Acknowledgments: This work was supported by the EU H2020 AI4Media No. 951911 project.

Table 6: Split 1

Image Source	Set	Generator
ImageNet [17]	Seen Real	-
GenImage [75]	Seen Fake	wukong [67] Midjourney [44] SD1.4 [66] VQDM [29]
	Unseen Fake	glide [48] ADM [19] SD1.5 [66] BigGAN [7]

A Supplementary Material

The supplementary material is organized as follows:

- In Appendix A.1, we provide additional details on the GenImage [75] dataset and the splits used for attribution.
- In Appendix A.2, we provide a frequency analysis on the images produced by each generator.
- In Appendix A.3, we provide an extended analysis on GAN-Generated image Attribution with standard deviations.
- In Appendix A.4, we provide the perturbation intensity intervals used for the robustness experiments.
- In Appendix A.5, we provide retrieval results on the GenImage [75] dataset using the k -NN approach described in the main paper.
- In Appendix A.6, provide a detailed explanation of the rejection strategies used for the linear probe classifier.

A.1 Additional details on GenImage dataset

We provide a full description of the five splits of the GenImage [75] dataset in Tab. 6, Tab. 7, Tab. 8, Tab. 9, and Tab. 10.

A.2 Frequency analysis

In Fig. 8 we show a frequency analysis of the noise residuals of each class of the GenImage dataset, using the denoising model and the pipeline described in [13]. While BigGAN shows the most peculiar traces, some Diffusion models (VQDM, glide, SD, Midjourney) still show visible artifacts in the frequency spectra, while others (ADM, wukong) show faint traces, almost indistinguishable from the frequency spectrum of real images.

Table 7: Split 2

Image Source	Set	Generator
ImageNet [17]	Seen Real	-
GenImage [75]	Seen Fake	Midjourney [44] SD1.4 [66] VQDM [29] BigGAN [7]
	Unseen Fake	wukong [67] glide [48] ADM [19] SD1.5 [66]

Table 8: Split 3

Image Source	Set	Generator
ImageNet [17]	Seen Real	-
GenImage [75]	Seen Fake	SD1.4 [66] VQDM [29] BigGAN [7] ADM [19]
	Unseen Fake	wukong [67] glide [48] SD1.5 [66] Midjourney [44]

A.3 Extended analysis on GAN Open Set Attribution

In Tab. 11, we present an extended analysis of GAN Open Set Attribution results using the OSMA [69] dataset. The analysis includes closed-set accuracy on Seen data as well as open-set AUC and OSCR across four configurations of Unseen data. For each entry, the table reports the mean performance across five splits, along with the standard deviation. All methods achieve over 90% accuracy on the closed-set, which consists of 15 classes, and demonstrate competitive open-set performance on three of the four Unseen data configurations (Unseen Architecture, Unseen Data, and Unseen All), with up to 64 total classes. However, the Unseen Seed configuration poses a significant challenge for all evaluated methods, and PRNU [43] and POSE [69] exhibit the highest performance in this scenario. Our method, which leverages high-level semantic features, struggles in distinguishing between Seen and Unseen data under this configuration. In contrast, PRNU [43] and [69], which utilize PRNU filters and low-level frequency information, are more responsive to the subtle traces left by model weights.

Table 9: Split 4

Image Source	Set	Generator
ImageNet [17]	Seen Real	-
GenImage [75]	Seen Fake	SD1.4 [66] VQDM [29] BigGAN [7] ADM [19]
	Unseen Fake	wukong [67] glide [48] SD1.5 [66] Midjourney [44]

Table 10: Split 5

Image Source	Set	Generator
ImageNet [17]	Seen Real	-
GenImage [75]	Seen Fake	SD1.5 [66] BigGAN [7] ADM [19] glide [48]
	Unseen Fake	wukong [67] SD1.4 [66] Midjourney [44] VQDM [29]

To enhance performance in this challenging setting, incorporating also low-level information from the initial layers of Vision Foundation Models could be beneficial—a direction we plan to explore in future work.

A.4 Perturbation intervals

In this section we provide the perturbation intervals used in robustness experiments. Each perturbation is randomly applied to the image with $p = 0.5$, and the perturbation intensity is randomly chosen within the interval.

A.5 Retrieval results

We provide retrieval results using the clip embeddings without the projection layer in Fig. 9. Results show that using a properly chosen intermediate layer we are able to access low-level information of the image related to texture, color and focus, along with higher-level information such as the pose and semantic content.

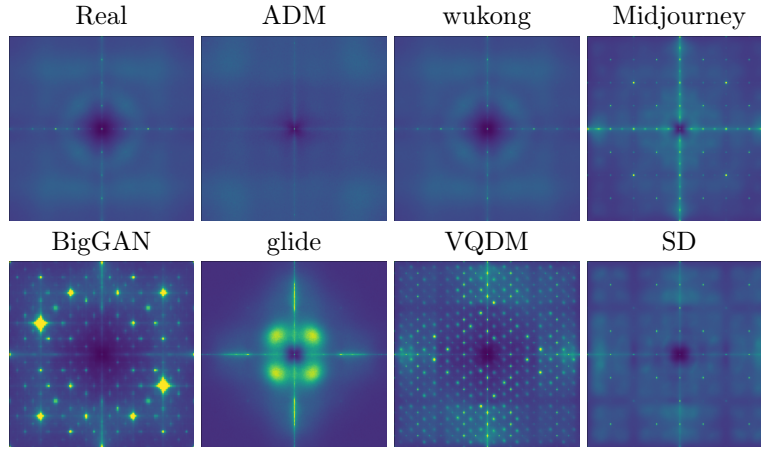


Fig. 8: Averaged frequency spectra of synthetic images produced by different generators in GenImage dataset obtained using the pipeline described in [14]

Table 11: GAN Open Set Origin Attribution on OSMA [69] dataset. We provide the results of three variants of our method: Nearest Neighbors (NN), Nearest Neighbors with trained projection (NN+) and Linear Probing (LP). Results are provided as the average on five splits \pm the standard deviation.

Split	Metric	Ours (NN)	Ours (NN+)	Ours (LP)
Seen	Acc.	94.18 \pm 3.68	95.31 \pm 4.24	97.29 \pm 2.35
Unseen Seed	AUC	57.62 \pm 2.00	56.18 \pm 7.42	54.15 \pm 5.21
	OSCR	56.69 \pm 2.29	54.04 \pm 7.06	54.00 \pm 5.07
Unseen Arch.	AUC	77.95 \pm 4.60	80.22 \pm 1.61	78.78 \pm 4.60
	OSCR	75.16 \pm 3.74	77.27 \pm 3.98	<u>78.12 \pm 5.07</u>
Unseen Data	AUC	90.60 \pm 6.80	<u>88.90 \pm 6.40</u>	90.60 \pm 4.39
	OSCR	91.77 \pm 5.21	85.42 \pm 8.60	<u>89.52 \pm 5.08</u>
Unseen All	AUC	80.42 \pm 1.11	<u>80.65 \pm 3.28</u>	79.29 \pm 3.68
	OSCR	77.11 \pm 3.40	78.22 \pm 3.28	<u>78.77 \pm 4.24</u>

A.6 Rejection strategies

One of the most simple strategies is using the maximum softmax probability (MSP) [32], which is the strategy used in POSE and in our main results. Other post-hoc methods, which require only the predictive distribution are MaxLogit [31], which uses the unnormalized logits instead of the softmax output, Energy [39] computes the soft maximum of the logits via LogSumExp, the Shannon Entropy and the Generalized Entropy [40]. We also evaluated methods that require access to the training features, such as virtual logit matching (ViM) [64], which incorpo-

Perturbation	Parameter	Min	Max
JPEG Compression	Quality	10	90
Gaussian Blur	Kernel size	3	15
Gaussian Noise	Variance	10	100
Brightness	Factor	-0.5	0.5
Contrast	Factor	0.5	2.0
Saturation	Factor	0.5	2.0
Rotation	Degrees	0	30

Table 12: Perturbation intervals

rates information from the training feature space and the predictive distribution by calculating a *residual* of the feature \mathbf{z} , $\|\mathbf{z}^{P\perp}\|$.

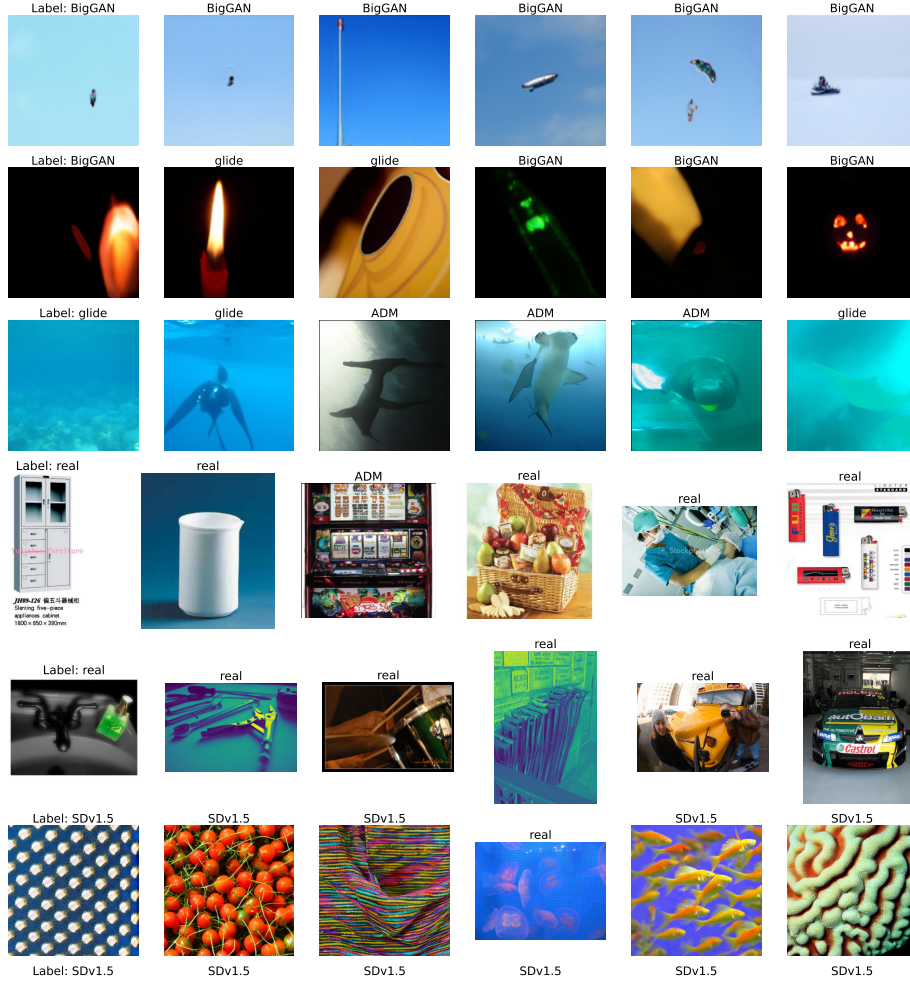


Fig. 9: Retrieval results on GenImage using not-projected CLIP embeddings

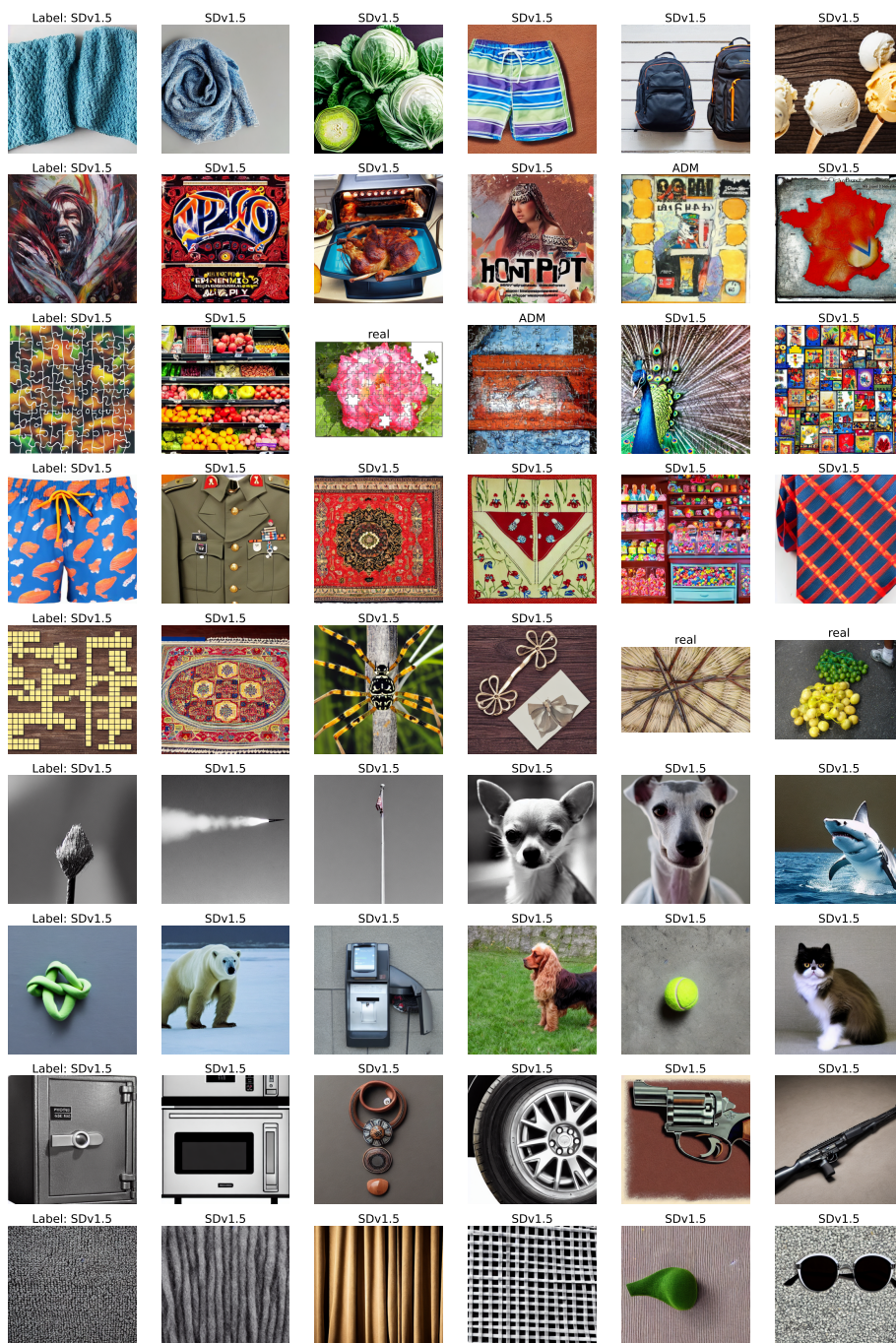


Fig. 9: Retrieval results on GenImage using not-projected CLIP embeddings

References

1. Amoroso, R., Morelli, D., Cornia, M., Baraldi, L., Del Bimbo, A., Cucchiara, R., et al.: Parents and children: Distinguishing multimodal deepfakes from natural images. *ACM TRANSACTIONS ON MULTIMEDIA COMPUTING, COMMUNICATIONS AND APPLICATIONS* (2024)
2. Barattin, S., Tzelepis, C., Patras, I., Sebe, N.: Attribute-preserving face dataset anonymization via latent code optimization. In: *Proceedings of the IEEE/CVF conference on computer vision and pattern recognition*. pp. 8001–8010 (2023)
3. Bounareli, S., Tzelepis, C., Argyriou, V., Patras, I., Tzimiropoulos, G.: Hyper-reenact: one-shot reenactment via jointly learning to refine and retarget faces. In: *Proceedings of the IEEE/CVF International Conference on Computer Vision*. pp. 7149–7159 (2023)
4. Bounareli, S., Tzelepis, C., Argyriou, V., Patras, I., Tzimiropoulos, G.: Stylemask: Disentangling the style space of stylegan2 for neural face reenactment. In: *2023 IEEE 17th international conference on automatic face and gesture recognition (FG)*. pp. 1–8. IEEE (2023)
5. Bounareli, S., Tzelepis, C., Argyriou, V., Patras, I., Tzimiropoulos, G.: Diffusionact: Controllable diffusion autoencoder for one-shot face reenactment. *arXiv preprint arXiv:2403.17217* (2024)
6. Bounareli, S., Tzelepis, C., Argyriou, V., Patras, I., Tzimiropoulos, G.: One-shot neural face reenactment via finding directions in gan’s latent space. *International Journal of Computer Vision* pp. 1–31 (2024)
7. Brock, A., Donahue, J., Simonyan, K.: Large scale gan training for high fidelity natural image synthesis. *arXiv preprint arXiv:1809.11096* (2018)
8. Bui, T., Yu, N., Collomosse, J.: RepMix: Representation Mixing for Robust Attribution of Synthesized Images. In: *Computer Vision – ECCV 2022: 17th European Conference, Tel Aviv, Israel, October 23–27, 2022, Proceedings, Part XIV*. pp. 146–163. Springer-Verlag, Berlin, Heidelberg (Oct 2022). https://doi.org/10.1007/978-3-031-19781-9_9, https://doi.org/10.1007/978-3-031-19781-9_9
9. Caron, M., Touvron, H., Misra, I., Jégou, H., Mairal, J., Bojanowski, P., Joulin, A.: Emerging properties in self-supervised vision transformers. In: *Proceedings of the IEEE/CVF international conference on computer vision*. pp. 9650–9660 (2021)
10. Chen, G., Peng, P., Wang, X., Tian, Y.: Adversarial reciprocal points learning for open set recognition. *IEEE Transactions on Pattern Analysis and Machine Intelligence* **44**(11), 8065–8081 (2021)
11. Cioni, D., Berlincioni, L., Becattini, F., Del Bimbo, A.: Diffusion based augmentation for captioning and retrieval in cultural heritage. In: *Proceedings of the IEEE/CVF International Conference on Computer Vision*. pp. 1707–1716 (2023)
12. Cocchi, F., Baraldi, L., Poppi, S., Cornia, M., Baraldi, L., Cucchiara, R.: Unveiling the impact of image transformations on deepfake detection: An experimental analysis. In: *International Conference on Image Analysis and Processing*. pp. 345–356. Springer (2023)
13. Corvi, R., Cozzolino, D., Poggi, G., Nagano, K., Verdoliva, L.: Intriguing properties of synthetic images: from generative adversarial networks to diffusion models. In: *Proceedings of the IEEE/CVF Conference on Computer Vision and Pattern Recognition*. pp. 973–982 (2023)
14. Corvi, R., Cozzolino, D., Zingarini, G., Poggi, G., Nagano, K., Verdoliva, L.: On The Detection of Synthetic Images Generated by Diffusion Models. In: *ICASSP*

- 2023 - 2023 IEEE International Conference on Acoustics, Speech and Signal Processing (ICASSP). pp. 1–5 (Jun 2023). <https://doi.org/10.1109/ICASSP49357.2023.10095167>, <https://ieeexplore.ieee.org/abstract/document/10095167>, ISSN: 2379-190X
15. Cozzolino, D., Poggi, G., Corvi, R., Nießner, M., Verdoliva, L.: Raising the bar of ai-generated image detection with clip (2023)
 16. DeepMind: Imagen2 (2023), <https://deepmind.google/technologies/imagen-2/>
 17. Deng, J., Dong, W., Socher, R., Li, L.J., Li, K., Fei-Fei, L.: Imagenet: A large-scale hierarchical image database. In: 2009 IEEE conference on computer vision and pattern recognition. pp. 248–255. Ieee (2009)
 18. Dhamija, A.R., Günther, M., Boulton, T.: Reducing Network Agnostophobia. In: Advances in Neural Information Processing Systems. vol. 31. Curran Associates, Inc. (2018), <https://proceedings.neurips.cc/paper/2018/hash/48db71587df6c7c442e5b76cc723169a-Abstract.html>
 19. Dhariwal, P., Nichol, A.: Diffusion models beat gans on image synthesis. Advances in neural information processing systems **34**, 8780–8794 (2021)
 20. D’Incà, M., Tzelepis, C., Patras, I., Sebe, N.: Improving fairness using vision-language driven image augmentation. In: Proceedings of the IEEE/CVF Winter Conference on Applications of Computer Vision. pp. 4695–4704 (2024)
 21. Dosovitskiy, A., Beyer, L., Kolesnikov, A., Weissenborn, D., Zhai, X., Unterthiner, T., Dehghani, M., Minderer, M., Heigold, G., Gelly, S., et al.: An image is worth 16x16 words: Transformers for image recognition at scale. arXiv preprint arXiv:2010.11929 (2020)
 22. Durall, R., Keuper, M., Keuper, J.: Watch Your Up-Convolution: CNN Based Generative Deep Neural Networks Are Failing to Reproduce Spectral Distributions. pp. 7890–7899 (2020), https://openaccess.thecvf.com/content_CVPR_2020/html/Durall_Watch_Your_Up-Convolution_CNN_Based_Generative_Deep_Neural_Networks_Are_CVPR_2020_paper.html
 23. Esser, P., Kulal, S., Blattmann, A., Entezari, R., Müller, J., Saini, H., Levi, Y., Lorenz, D., Sauer, A., Boesel, F., et al.: Scaling rectified flow transformers for high-resolution image synthesis. In: Forty-first International Conference on Machine Learning (2024)
 24. Fernandez, P., Couairon, G., Jégou, H., Douze, M., Furon, T.: The Stable Signature: Rooting Watermarks in Latent Diffusion Models. pp. 22466–22477 (2023), https://openaccess.thecvf.com/content/ICCV2023/html/Fernandez_The_Stable_Signature_Rooting_Watermarks_in_Latent_Diffusion_Models_ICCV_2023_paper.html
 25. Frank, J., Eisenhofer, T., Schönherr, L., Fischer, A., Kolossa, D., Holz, T.: Leveraging frequency analysis for deep fake image recognition. In: International conference on machine learning. pp. 3247–3258. PMLR (2020)
 26. Frank, J., Eisenhofer, T., Schönherr, L., Fischer, A., Kolossa, D., Holz, T.: Leveraging Frequency Analysis for Deep Fake Image Recognition. In: Proceedings of the 37th International Conference on Machine Learning. pp. 3247–3258. PMLR (Nov 2020), <https://proceedings.mlr.press/v119/frank20a.html>, ISSN: 2640-3498
 27. Gadre, S.Y., Ilharco, G., Fang, A., Hayase, J., Smyrnis, G., Nguyen, T., Marten, R., Wortsman, M., Ghosh, D., Zhang, J., Orgad, E., Entezari, R., Daras, G., Pratt, S., Ramanujan, V., Bitton, Y., Marathe, K., Musmann, S., Vencu, R., Cherti, M., Krishna, R., Koh, P.W., Saukh, O., Ratner, A., Song, S., Hajishirzi, H., Farhadi, A., Beaumont, R., Oh, S., Dimakis, A., Jitsev, J., Carmon, Y., Shankar, V., Schmidt, L.: Datacomp: In search of the next generation of multimodal datasets (2023), <https://arxiv.org/abs/2304.14108>

28. Girish, S., Suri, S., Rambhatla, S.S., Shrivastava, A.: Towards Discovery and Attribution of Open-World GAN Generated Images. pp. 14094–14103 (2021), https://openaccess.thecvf.com/content/ICCV2021/html/Girish_Towards_Discovery_and_Attribution_of_Open-World_GAN_Generated_Images_ICCV_2021_paper.html
29. Gu, S., Chen, D., Bao, J., Wen, F., Zhang, B., Chen, D., Yuan, L., Guo, B.: Vector quantized diffusion model for text-to-image synthesis. In: Proceedings of the IEEE/CVF Conference on Computer Vision and Pattern Recognition. pp. 10696–10706 (2022)
30. He, K., Zhang, X., Ren, S., Sun, J.: Deep residual learning for image recognition. In: Proceedings of the IEEE conference on computer vision and pattern recognition. pp. 770–778 (2016)
31. Hendrycks, D., Basart, S., Mazeika, M., Zou, A., Kwon, J., Mostajabi, M., Steinhardt, J., Song, D.: Scaling Out-of-Distribution Detection for Real-World Settings (May 2022). <https://doi.org/10.48550/arXiv.1911.11132>, <http://arxiv.org/abs/1911.11132>, arXiv:1911.11132 [cs]
32. Hendrycks, D., Gimpel, K.: A Baseline for Detecting Misclassified and Out-of-Distribution Examples in Neural Networks (Oct 2018). <https://doi.org/10.48550/arXiv.1610.02136>, <http://arxiv.org/abs/1610.02136>, arXiv:1610.02136 [cs]
33. Huang, R., Geng, A., Li, Y.: On the importance of gradients for detecting distributional shifts in the wild. *Advances in Neural Information Processing Systems* **34**, 677–689 (2021)
34. Khosla, P., Teterwak, P., Wang, C., Sarna, A., Tian, Y., Isola, P., Maschinot, A., Liu, C., Krishnan, D.: Supervised contrastive learning. arXiv preprint arXiv:2004.11362 (2020)
35. Kim, C., Ren, Y., Yang, Y.: Decentralized Attribution of Generative Models (Oct 2020), https://openreview.net/forum?id=_kxlvvh0odK
36. Laszkiewicz, M., Ricker, J., Lederer, J., Fischer, A.: Single-Model Attribution of Generative Models Through Final-Layer Inversion (Feb 2024). <https://doi.org/10.48550/arXiv.2306.06210>, <http://arxiv.org/abs/2306.06210>, arXiv:2306.06210 [cs]
37. Lee, K., Lee, K., Lee, H., Shin, J.: A simple unified framework for detecting out-of-distribution samples and adversarial attacks. *Advances in neural information processing systems* **31** (2018)
38. Liu, D.C., Nocedal, J.: On the limited memory bfgs method for large scale optimization. *Mathematical programming* **45**(1), 503–528 (1989)
39. Liu, W., Wang, X., Owens, J., Li, Y.: Energy-based Out-of-distribution Detection. In: *Advances in Neural Information Processing Systems*. vol. 33, pp. 21464–21475. Curran Associates, Inc. (2020), <https://proceedings.neurips.cc/paper/2020/hash/f5496252609c43eb8a3d147ab9b9c006-Abstract.html>
40. Liu, X., Lochman, Y., Zach, C.: GEN: Pushing the Limits of Softmax-Based Out-of-Distribution Detection. pp. 23946–23955 (2023), https://openaccess.thecvf.com/content/CVPR2023/html/Liu_GEN_Pushing_the_Limits_of_Softmax-Based_Out-of-Distribution_Detection_CVPR_2023_paper.html
41. Ma, R., Duan, J., Kong, F., Shi, X., Xu, K.: Exposing the fake: Effective diffusion-generated images detection. arXiv preprint arXiv:2307.06272 (2023)
42. Marimont, S.N., Baugh, M., Siomos, V., Tzelepis, C., Kainz, B., Tarroni, G.: Disyre: Diffusion-inspired synthetic restoration for unsupervised anomaly detection. arXiv preprint arXiv:2311.15453 (2023)

43. Marra, F., Gagnaniello, D., Verdoliva, L., Poggi, G.: Do GANs Leave Artificial Fingerprints? In: 2019 IEEE Conference on Multimedia Information Processing and Retrieval (MIPR). pp. 506–511 (Mar 2019). <https://doi.org/10.1109/MIPR.2019.00103>, https://ieeexplore.ieee.org/abstract/document/8695364?casa_token=r1bBONM3NQ4AAAAA:K800F8bB0AnM26B9Ip15YU8-zJ5D5wnQVRVn0JUgnwKhWOLBFpFDvKYNnw1eU2U_Rbbi1sWC
44. Midjourney: <https://www.midjourney.com> (2022)
45. Morelli, D., Baldrati, A., Cartella, G., Cornia, M., Bertini, M., Cucchiara, R.: LaDI-VTON: Latent Diffusion Textual-Inversion Enhanced Virtual Try-On. In: Proceedings of the ACM International Conference on Multimedia (2023)
46. Naval Marimont, S., Siomos, V., Baugh, M., Tzelepis, C., Kainz, B., Tarroni, G.: Ensembled cold-diffusion restorations for unsupervised anomaly detection. arXiv e-prints pp. arXiv–2407 (2024)
47. Neal, L., Olson, M., Fern, X., Wong, W.K., Li, F.: Open set learning with counterfactual images. In: Proceedings of the European conference on computer vision (ECCV). pp. 613–628 (2018)
48. Nichol, A., Dhariwal, P., Ramesh, A., Shyam, P., Mishkin, P., McGrew, B., Sutskever, I., Chen, M.: Glide: Towards photorealistic image generation and editing with text-guided diffusion models. arXiv preprint arXiv:2112.10741 (2021)
49. Ojha, U., Li, Y., Lee, Y.J.: Towards Universal Fake Image Detectors that Generalize Across Generative Models (Feb 2023), <http://arxiv.org/abs/2302.10174>, arXiv:2302.10174 [cs]
50. Oldfield, J., Tzelepis, C., Panagakis, Y., Nicolaou, A., Patras, I., et al.: Panda: Unsupervised learning of parts and appearances in the feature maps of gans (2023)
51. Oldfield, J., Tzelepis, C., Panagakis, Y., Nicolaou, M., Patras, I.: Parts of speech-grounded subspaces in vision-language models. Advances in Neural Information Processing Systems **36**, 2700–2724 (2023)
52. Oldfield, J., Tzelepis, C., Panagakis, Y., Nicolaou, M.A., Patras, I.: Bilinear models of parts and appearances in generative adversarial networks. IEEE Transactions on Pattern Analysis and Machine Intelligence (2024)
53. Oquab, M., Darcet, T., Moutakanni, T., Vo, H., Szafraniec, M., Khalidov, V., Fernandez, P., Haziza, D., Massa, F., El-Nouby, A., Assran, M., Ballas, N., Galuba, W., Howes, R., Huang, P.Y., Li, S.W., Misra, I., Rabbat, M., Sharma, V., Synnaeve, G., Xu, H., Jegou, H., Mairal, J., Labatut, P., Joulin, A., Bojanowski, P.: DINOv2: Learning Robust Visual Features without Supervision (Feb 2024). <https://doi.org/10.48550/arXiv.2304.07193>, <http://arxiv.org/abs/2304.07193>, arXiv:2304.07193 [cs]
54. Radford, A., Kim, J.W., Hallacy, C., Ramesh, A., Goh, G., Agarwal, S., Sastry, G., Askell, A., Mishkin, P., Clark, J., Krueger, G., Sutskever, I.: Learning Transferable Visual Models From Natural Language Supervision. In: Proceedings of the 38th International Conference on Machine Learning. pp. 8748–8763. PMLR (Jul 2021), <https://proceedings.mlr.press/v139/radford21a.html>, iSSN: 2640-3498
55. Ramesh, A., Pavlov, M., Goh, G., Gray, S., Voss, C., Radford, A., Chen, M., Sutskever, I.: Zero-shot text-to-image generation. In: International conference on machine learning. pp. 8821–8831. Pmlr (2021)
56. Ricker, J., Lukovnikov, D., Fischer, A.: Aeroblade: Training-free detection of latent diffusion images using autoencoder reconstruction error. In: Proceedings of the IEEE/CVF Conference on Computer Vision and Pattern Recognition (CVPR). pp. 9130–9140 (June 2024)

57. Schuhmann, C., Beaumont, R., Vencu, R., Gordon, C., Wightman, R., Cherti, M., Coombes, T., Katta, A., Mullis, C., Wortsman, M., et al.: Laion-5b: An open large-scale dataset for training next generation image-text models. *Advances in Neural Information Processing Systems* **35**, 25278–25294 (2022)
58. Sha, Z., Li, Z., Yu, N., Zhang, Y.: DE-FAKE: Detection and Attribution of Fake Images Generated by Text-to-Image Generation Models. In: *Proceedings of the 2023 ACM SIGSAC Conference on Computer and Communications Security*. pp. 3418–3432. CCS '23, Association for Computing Machinery, New York, NY, USA (Nov 2023). <https://doi.org/10.1145/3576915.3616588>, <https://dl.acm.org/doi/10.1145/3576915.3616588>
59. Song, Y., Shen, L., Xing, L., Ermon, S.: Solving inverse problems in medical imaging with score-based generative models. In: *International Conference on Learning Representations*
60. Thomee, B., Shamma, D.A., Friedland, G., Elizalde, B., Ni, K., Poland, D., Borth, D., Li, L.J.: Yfcc100m: The new data in multimedia research. *Communications of the ACM* **59**(2), 64–73 (2016)
61. Tzelepis, C., Oldfield, J., Tzimiropoulos, G., Patras, I.: Contraclip: Interpretable gan generation driven by pairs of contrasting sentences. *arXiv preprint arXiv:2206.02104* (2022)
62. Tzelepis, C., Tzimiropoulos, G., Patras, I.: Warpedganspace: Finding non-linear rbf paths in gan latent space. In: *Proceedings of the IEEE/CVF international conference on computer vision*. pp. 6393–6402 (2021)
63. Vaze, S., Han, K., Vedaldi, A., Zisserman, A.: Open-Set Recognition: a Good Closed-Set Classifier is All You Need? (Apr 2022). <https://doi.org/10.48550/arXiv.2110.06207>, <http://arxiv.org/abs/2110.06207>, arXiv:2110.06207 [cs]
64. Wang, H., Li, Z., Feng, L., Zhang, W.: ViM: Out-of-Distribution With Virtual-Logit Matching. pp. 4921–4930 (2022), https://openaccess.thecvf.com/content/CVPR2022/html/Wang_ViM_Out-of-Distribution-With-Virtual-Logit-Matching_CVPR2022_paper.html
65. Wang, Z., Chen, C., Zeng, Y., Lyu, L., Ma, S.: Where Did I Come From? Origin Attribution of AI-Generated Images (Nov 2023), <https://openreview.net/forum?id=g8bjq0qx0l>
66. WebUI, S.D.: <https://github.com/AUTOMATIC111/stable-diffusion-webui> (2022)
67. Wukong: <https://xihe.mindspore.cn/modelzoo/wukong> (2022)
68. Yang, T., Huang, Z., Cao, J., Li, L., Li, X.: Deepfake Network Architecture Attribution. *Proceedings of the AAAI Conference on Artificial Intelligence* **36**(4), 4662–4670 (Jun 2022). <https://doi.org/10.1609/aaai.v36i4.20391>, <https://ojs.aaai.org/index.php/AAAI/article/view/20391>, number: 4
69. Yang, T., Wang, D., Tang, F., Zhao, X., Cao, J., Tang, S.: Progressive Open Space Expansion for Open-Set Model Attribution. pp. 15856–15865 (2023), https://openaccess.thecvf.com/content/CVPR2023/html/Yang_Progressive_Open_Space_Expansion_for_Open-Set_Model_Attribution_CVPR_2023_paper.html
70. Yu, N., Davis, L.S., Fritz, M.: Attributing Fake Images to GANs: Learning and Analyzing GAN Fingerprints. pp. 7556–7566 (2019), https://openaccess.thecvf.com/content_ICCV_2019/html/Yu_Attributing_Fake_Images_to_GANs_Learning_and_Analyzing_GAN_Fingerprints_ICCV_2019_paper.html
71. Yu, N., Skripniuk, V., Abdelnabi, S., Fritz, M.: Artificial Fingerprinting for Generative Models: Rooting Deepfake Attribution in Training Data. pp. 14448–14457 (2021), https://openaccess.thecvf.com/content_ICCV2021/html/

- Yu_Artificial_Fingerprinting_for_Generative_Models_Rooting_Deepfake_Attribution_in_Training_ICCV_2021_paper.html
72. Yu, N., Skripniuk, V., Chen, D., Davis, L.S., Fritz, M.: Responsible Disclosure of Generative Models Using Scalable Fingerprinting (Oct 2021), <https://openreview.net/forum?id=s0K-zS6WHB>
 73. Zhang, X., Karaman, S., Chang, S.F.: Detecting and simulating artifacts in gan fake images. In: 2019 IEEE international workshop on information forensics and security (WIFS). pp. 1–6. IEEE (2019)
 74. Zhu, M., Chen, H., Huang, M., Li, W., Hu, H., Hu, J., Wang, Y.: GenDet: Towards Good Generalizations for AI-Generated Image Detection (Dec 2023). <https://doi.org/10.48550/arXiv.2312.08880>, <http://arxiv.org/abs/2312.08880>, arXiv:2312.08880 [cs]
 75. Zhu, M., Chen, H., Yan, Q., Huang, X., Lin, G., Li, W., Tu, Z., Hu, H., Hu, J., Wang, Y.: GenImage: A Million-Scale Benchmark for Detecting AI-Generated Image. *Advances in Neural Information Processing Systems* **36**, 77771–77782 (Dec 2023), https://proceedings.neurips.cc/paper_files/paper/2023/hash/f4d4a021f9051a6c18183b059117e8b5-Abstract-Datasets_and_Benchmarks.html
 76. Özbey, M., Dalmaz, O., Dar, S.U.H., Bedel, H.A., Öztürk, S., Güngör, A., Çukur, T.: Unsupervised medical image translation with adversarial diffusion models. *IEEE Transactions on Medical Imaging* **42**(12), 3524–3539 (2023). <https://doi.org/10.1109/TMI.2023.3290149>